Satellite Type Estination from Ground-based Photometric Observation

Takao Endo, HItomi Ono, Jiro Suzuki and Toshiyuki Ando

Mitsubishi Electric Corporation, Information Technology R&D Center

Takashi Takanezawa

Mitsubishi Electric Corporation, Communication Systems Center

ABSTRACT

The optical photometric observation is potentially a powerful tool for understanding of the Geostationary Earth Orbit (GEO) objects. At first, we measured in laboratory the surface reflectance of common satellite materials, for example, Multi-layer Insulation (MLI), mono-crystalline silicon cells, and Carbon Fiber Reinforced Plastic (CFRP). Next, we calculated visual magnitude of a satellite by simplified shape and albedo. In this calculation model, solar panels have dimensions of 2 by 8 meters, and the bus area is 2 meters squared with measured optical properties described above. Under these conditions, it clarified the brightness can change the range between 3 and 4 magnitudes in one night, but color index changes only from 1 to 2 magnitudes. Finally, we observed the color photometric data of several GEO satellites visible from Japan multiple times in August and September 2014. We obtained that light curves of GEO satellites recorded in the B and V bands (using Johnson filters) by a ground-base optical telescope. As a result, color index changed approximately from 0.5 to 1 magnitude in one night, and the order of magnitude was not changed in all cases. In this paper, we briefly discuss about satellite type estimation using the relation between brightness and color index obtained from the photometric observation.

1. INTRODUCTION

Space Situational Awareness (SSA) is a concept about security in the outer space, in order to ensure the safety of the space flight, understand the current status of the satellites, prevent collision, or understand the status of the space debris, etc. Mainly, motion of the space debris observed by radio wave (radar) and optic (telescope), and then cataloged as the orbital elements. On the other hand, optical properties other than motion of the debris, such as luminance, time variation of luminance, or color index, are considered as useful information to guess the size, materials, and rotation of the target.

In previous research, variation of the bus of the GEO satellite is classified using magnitude and color index[1]. We observed the color photometric data of several GEO satellites visible from Japan using a ground-base telescope and bandpass filters. In this paper, we confirm repeatability by multiple observation, and discuss about satellite type estimation using the relation between brightness and color index obtained from the photometric observation.

2. ANALYSIS

2.1. THE SURFACE REFLECTANCE OF COMMON SATELLITE MATERIALS

As the artificial satellites shine brightly by mainly reflection of sunlight, it is important to know the spectral reflectance of typical materials of artificial satellites. At first, we obtained samples of Multi layer Insulation (MLI), mono-crystalline silicon cells (solar panel), and Carbon Fiber Reinforced Plastic (CFRP), and then measured the spectral reflectances. The measured samples are listed in table 1.

In figure 1, we plot the logarithm of the spectral reflectivity [%] against wave length λ [nm] for the samples in table 1. The incident angle to the normal of sample plane is set to 15 [°]. The broken lines, dot-dashed lines and solid lines

Table 1: Sample list

Sample	Surface characteristics
Multi layer Insulation (MLI)	Gold & silver, smooth surface
Mono-crystalline Silicon Cells (solar panel)	Black, smooth surface
Carbon Fiber Reinforced Plastic (CFRP)	Black, rough surface

show the s-polarized, p-polarized and averaged light, respectively. The transmittance of Johnson's UBVRI bandpass filter is plotted as dotted lines. Johnson filter will be discussed later in section 3.1. And yellow lines, blue lines, black lines show the reflectance of MLI, solar panel and CFRP, respectively.

From the figure 1, we can see that the reflectance of MLI is in proportion to the wave length in BV band. The solar panel, on the other hand, is inverse proportion to the wave length in BV band. The data of solar panel are intentionally hidden in R band because the characteristic feature is seen in this sample. This is probably due to the surface material of the multilayer coatings. If there is a characteristic structure in the optical spectrum of the satellite materials, photometric observation may enable easy classification.

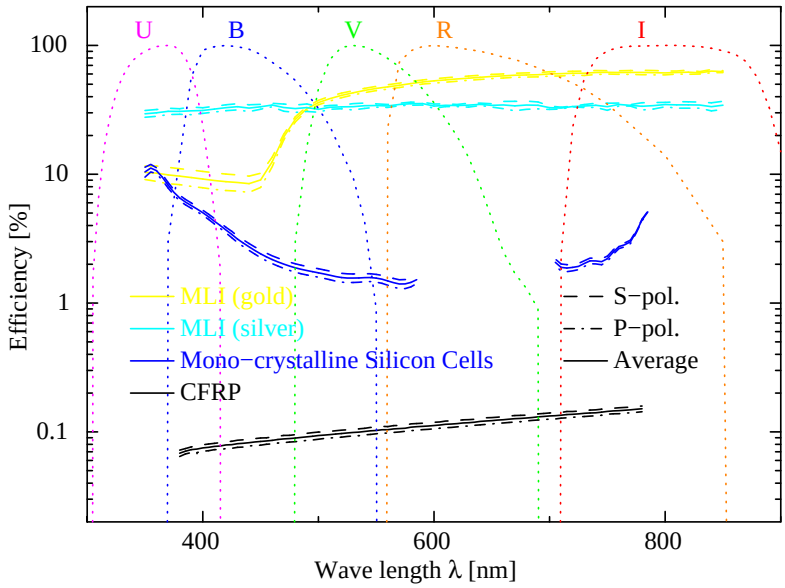

Fig. 1. Spectral reflectance of typical materials

2.2. LIGHT CURVE AND PROBABILITY DISTRIBUTION

Since the surface reflectances of the most common satellite materials are obtained, we next calculate the visual magnitude of the artificial satellites. First, we assume that the shape of satellites are basically made of two facets: a bus cube that is covered with MLI, and two solar panels which are placed at the each sides of the bus. Also all simulated reflections are diffuse. No specular reflections are taken into account.

Figure 2 shows the definition of coordinate system. The observer is located at the origin, x-axis is from the observer toward the satellite. The width and height of the bus of the satellite is a meters cube. The each flat plane in the paper

is defined as 1, 2, 3, 4, and the satellite angle θ is defined as the angle between normal to the plane 1 and x-axis. In the same way, the sun angle ϕ is defined as the angle between the sun and x-axis. r_s is the distance between the observer and the satellite, $r_\odot$ is the distance between the observer and the sun, and l is the distance between the sun and the satellite. In order to simplify the calculation, we ignore the effect of atmospheric absorption in this work.

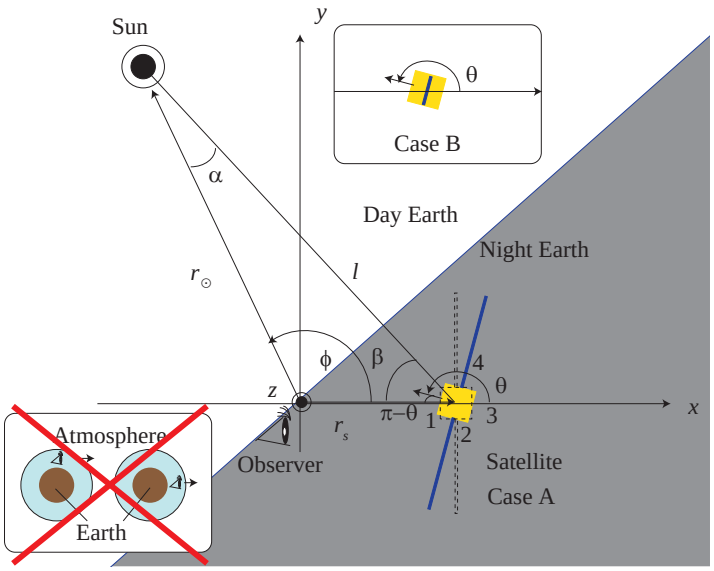

Fig. 2. The definition of coordinate system

Next, we defined that length of the short sides of the solar panel is a, the long sides is b, and the thickness is extremely thin. This panel is placed at the center of the bus $(a/2)$. We consider two cases of the motion of the artificial satellite as follows. Case A: The solar panel make a shadow over the bus, Case B: The solar panel doesn't make a shadow over the bus.

The artificial satellites, usually in order to generate electric power, adjust the solar panel toward the sun. We suppose the angle of the satellite θ less than ± 20 [°] from the solar angle ϕ, and then calculate the light curve of each bands (described by visual magnitude), color indexes, and the probability distributions.

Here, as a typical result, the light curves with the photometric filter B, V are shown in the figure 3. The upper panel in figure 3 shows the expected magnitude in B and V band, and lower panel also shows the expected color index B-V. The horizontal axis shows the solar angle ϕ in each panel. The blue lines and green lines show the B band and V band magnitude, respectively. The broken lines, dotted lines, and solid lines show the visual magnitude of the solar panel, the bus, and the total flux, respectively. The brightness can change the range between 3 and 4 magnitudes in one night according to the position of the sun, the satellite, and the observer. On the other hand, color index changes within only from 1 to 2 magnitudes.

Next, the probability density distribution is shown in figure 4. The probability [%] are plotted against the visual magnitudes for U, B, V, R and I bands. In this model, the probability in 11-12 magnitudes is the largest, however the results depend both on the size of the bus and solar panels, and on the surface reflectance of satellite materials.

In spite of the simplified model, we could estimate the visual magnitudes and the color index of the artificial satellite. After we prepare the observational instruments, we next plan to observe GEO satellites visible from Japan using a ground-base telescope.

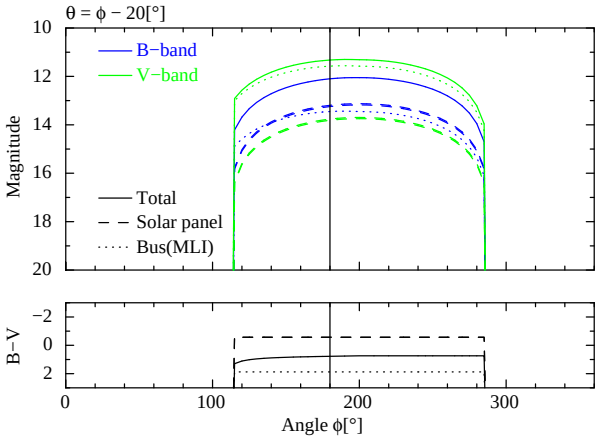

Fig. 3. Light curves (Case A, $\theta = \phi - 20$ [°])

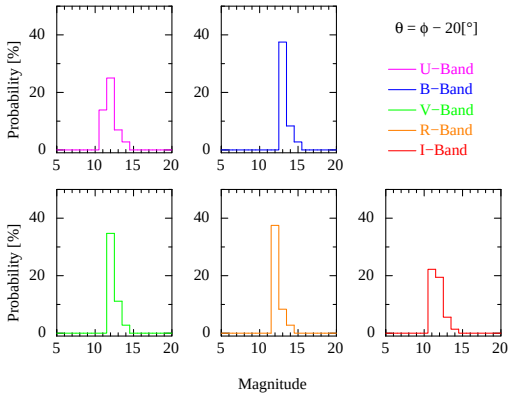

Fig. 4. Probability density functions

3. OBSERVATIONS OF GEO SATELLITES

3.1. INSTRUMENTATION

Summary of the observational instruments are listed in table 2. We use the diameter 280 mmϕ optical telescope, CCD camera, and the spectral filter. Here, in order to compare the previous works, we use Johnson's $UBVRI$ bandpass filters as a spectral filter[2]. It should be noted, if we use bandpass filter, only the selected wavelength band is transmitted. For example, equally divided by 5 colors, the energy flux per one color is $1/5$ of the original. For this reason, the larger telescope is better to perform the color photometric analysis.

Table 2: Summary of the observational instruments

Item	Specification
Telescope	C11AL-XLT (Celestron)
Focal length / aparture diameter	2800 [mm]/280 [mm]
Equatorial mount	AXD equatorial mount (Vixen)
CCD Camera	ST-im (SBIG)
Pixel format,size	648×486, 7.4 [μm]
Spectral filter	Johnson B & V bandpass (Baader planetarium)

3.2. SOURCE FLUX ESTIMATION

In order to estimate the source flux, the integration radius should be determined from the spread of the point source. The example images of GEO satellite with the integration radius are shown in figure 5. Figure 5 shows the intensity distribution in V band by contour after subtracting background. The red broken line, and the red solid line show the inner radius $r = 10$ [pixel] and outer radius $r = 20$ [pixel], respectively. Figure 5(a) is the example of observation at Aug. 20 0:44:43 (JST), and figure 5(b) at Aug. 20 0:52:27(JST).

Also, the vertical section of the center is shown in the right of the figure, and the horizontal section of the center is shown in the bottom of the figure. Comparing both the image and the sectional view in figure 5(a)-(b), the spread of

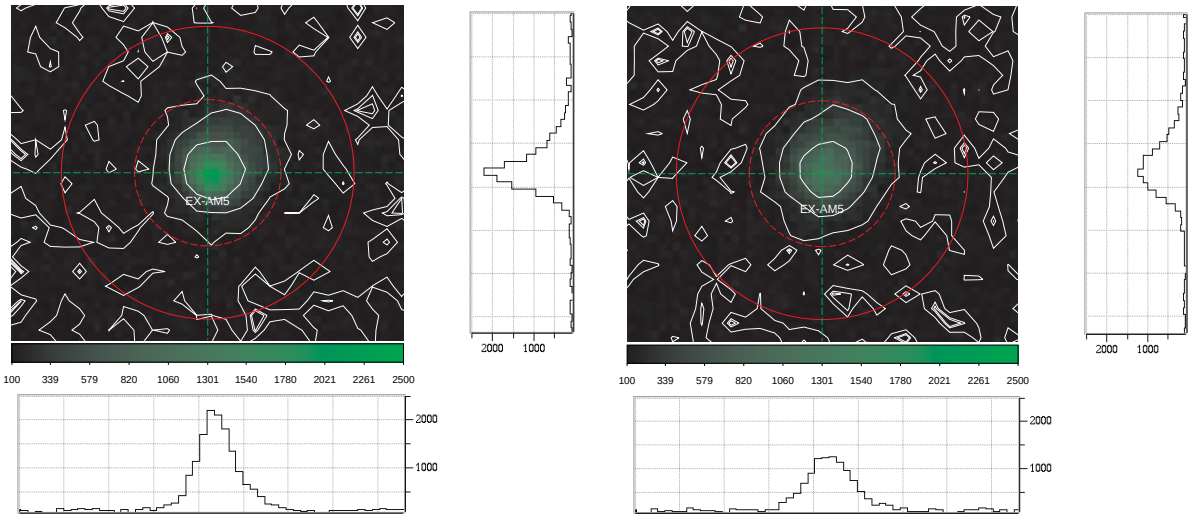

(a) Aug. 20 0:44:43 (b) Aug. 20 0:52:27

Fig. 5. Example images of Express-AM5

the image is significantly changed within about 8 minutes. In this example, as the total amount of source flux is slightly decreased, it indicates that the source flux is absorbed by a thin cloud or widely spread by atmospheric seeing. In any case, if the integrating radius is appropriately determined, the source flux can be estimated except for the absorption by the cloud.

3.3. OBSERVATION

In this section, we carry out the photometric observation of the artificial satellite in GEO above Japan by ground-base telescope. The observation target is the weather satellite Himawari, and the satellites around it. The image of Himawari, which is open to the public, is useful to make an observation plan. Because the location of the observation is hidden in the image of Himawari, Himawari may be difficult to be detected from the ground observer. The observation dates are from 0 a.m. to sunrise on Aug. 20, Aug. 22, and Sep. 27, JST (Japan Standard Time).

First, we subtract the background from the observed image, and correct the transmittance of the photometric filter and the quantum efficiency of CCD, then convert into the visual magnitudes. The light curve of the artificial satellite is shown in the figure 6. The blue lines and green lines in figure 6 show the visual magnitude in B band, and V band, respectively. Figure 6(a) is observed in the order of Chinasat-6A, Himawari-6, Express-AM5, Express-AT2, Chinasat-6A, Himawari-6, FY-2F, and figure 6(d) is observed in the order of Chinasat-6A, Express-AM5, Himawari-6, Express-AT2, Chinasat-6A. It should be noted, Chinasat-6A can't be detected in during 23:58-01:04, because the sun light which illuminates the satellite is totally eclipsed by the earth.

Next, we investigate the characteristics of the light curves of each artificial satellites, because the artificial satellites were observed for multiple times in different date. The light curves of each satellite are shown in figure 7. The figure 7(a) is the light curve of Himawari-6 after subtracting background. The blue lines and green lines show the visual magnitude of B and V band. Open triangles $\triangle$, small filled triangles ▲, and large filled triangles ▲ show the visual magnitude obtained at Aug. 20, Aug. 22 and Sep. 27, respectively.

In order to estimate the continuous light curve, the data points are fitted with a second or higher order polynomial for

Table 3: Typical magnitude and Color index

Target	Time (JST*)	V	B	B-V
Himawari-6	8/20 0:23:02	10.74	11.59	0.86
	8/20 3:10:05	11.41	12.29	0.88
	8/20 3:38:52	11.56	12.70	1.14
	8/22 23:05:16	11.35	11.92	0.58
	9/27 3:25:55	11.61	12.31	0.70
Express-AM5	8/20 01:00:29	9.939	10.51	0.57
	8/20 01:50:53	10.22	11.07	0.85
	8/20 02:00:01	10.38	11.11	0.73
	8/22 23:57:07	10.66	11.38	0.71
	9/27 03:25:55	11.06	11.70	0.64
Express-AT2	8/20 01:32:10	12.15	12.93	0.77
	8/23 00:54:43	11.89	12.68	0.79
	9/27 01:40:19	12.78	14.46	1.68
Chinasat-6A	8/19 22:35;46	11.04	12.41	1.38
	8/20 02:25:26	10.70	12.14	1.45
	9/26 22:54:49	10.88	12.31	1.43
	9/26 23:19:41	10.52	12.17	1.66
	9/26 23:23:27	10.49	11.87	1.38
	9/26 23:54:35	10.18	11.58	1.40
	9/27 02:49:55	10.78	11.75	0.97
	9/27 03:02:53	10.70	11.73	1.03
	9/27 04:01:55	10.35	11.08	0.73

$*$ JST: Japan Standard Time

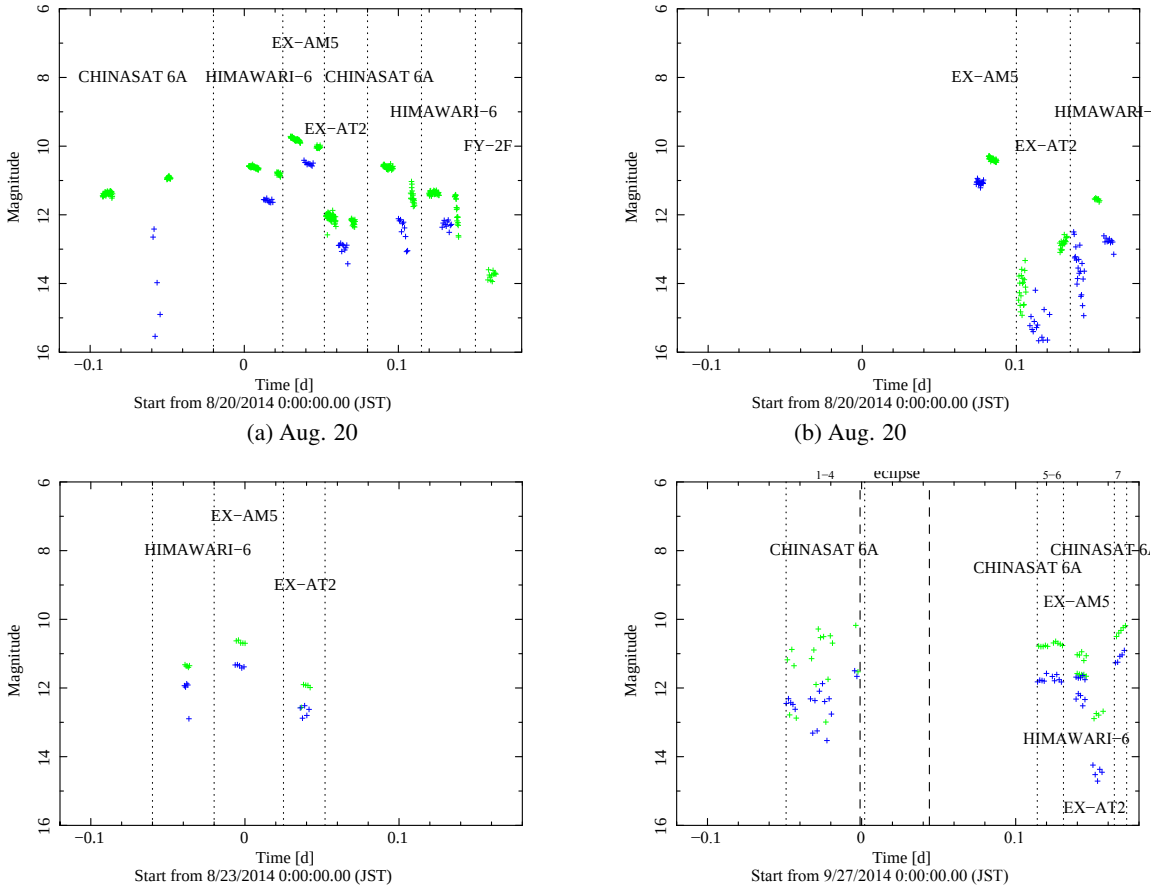

(a) Aug. 20 (b) Aug. 20

(c) Aug. 22 (d) Sep. 27

Fig. 6. Light curves after subtracting background (Aug. 20, Aug. 22 and Sep. 27)

all observations. The solid lines in figure 7 show the best-fit second-order polynomial. In the same way, the broken lines show the best-fit third-order polynomial.

The figure 7(b) shows the light curve of Express-AM5 same as figure 7(a) Also, open stars ⋆, small filled stars ★, and large filled stars ★ show the visual magnitude obtained at Aug. 20, Aug. 22 and Sep. 27, respectively. The broken lines in figure 7 show the best-fit third-order polynomial.

The next figure 7(c) shows the light curve of Express-AT2 same as figure 7(a) Open squares □, small filled squares ■, and large filled squares ■ show the visual magnitude obtained at Aug. 20, Aug. 22 and Sep. 27, respectively.

The last figure 7(d) shows the light curve of the Chinasat 6A same as fugure 7(a) Open circles ○, and large filled circles • show the visual magnitude obtained at Aug. 20 and Sep. 27, respectively. Chinasat-6A can't be detected in during 23:58-01:04, because of assuming eclipse. However, we carry out the fitting for all observations to investigate the sun angle dependence of the light curve. The broken lines in figure 7(d) show the best-fit 3rd order polynomial extrapolated during eclipse.

From the light curves of the each artificial satellites in figure 7, it is confirmed that there is no extreme fluctuation, excluding an eclipse and significant absorption due to clouds. This is also expected by the calculated light curve as shown in figure 3. The tendency such as (1) the peak is around at the center of the light curve, (2) the visual magnitude in B band is fainter than that of V band, are same as the model, but the values were not matched yet to the simulated

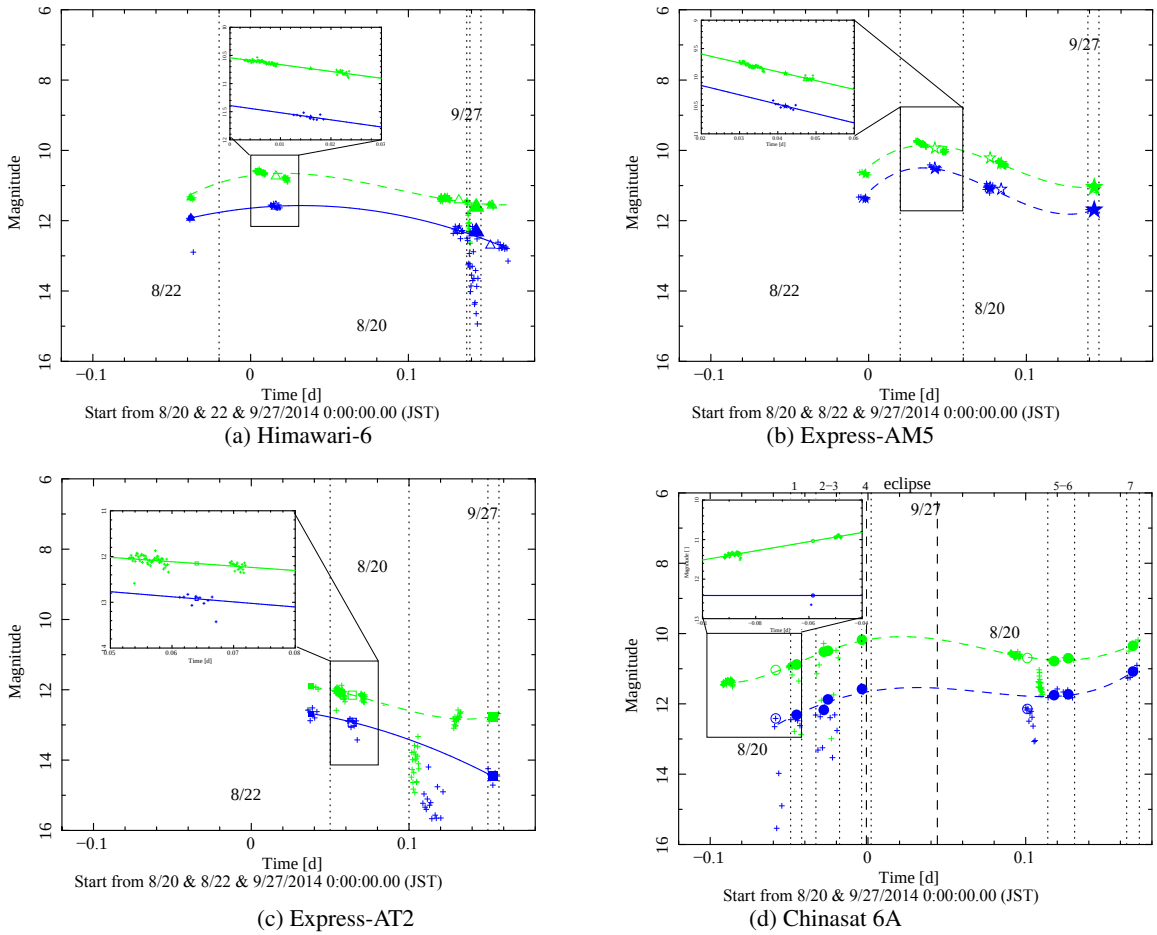

Fig. 7. Light curves of GEO satellites.

one. We consider that the difference between calculation and observation caused by (1) the size of the satellites, (2) the geometry of the satellites, and (3) the spectral reflection characteristic of each surface.

4. DISCUSSION

In the previous section, we obtained the photometric information of GEO satellites. We next try to explain the classification of the artificial satellites. Figure 8 shows the color index versus the visual magnitude diagram called color-magnitude diagram (CMD). In the figure 8, the flux in V band is increasing from bottom to top. On the contrary, the flux in B band is decreasing from bottom to top. Also, it is brighter towards the left side, and fainter towards the right side. The color index of the solar shows the horizontal broken line, and the calculation model (refer section 2.2) is represented by the dotted line and dashed line. The different symbols refer to each satellites listed in table 3.

From the figure 8, we can see that the variation of the color index is about $\sim$ 0.5 magnitude for Himawari-6, and about $\sim$ 1 magnitude for Express-AM5, Express-AT2, and Chinasat-6A. Also, it is confirmed that the order of the bright satellites are Express-AM5, Himawari-6, and Express-AT2, and the order of magnitude in all case is not clearly changed.

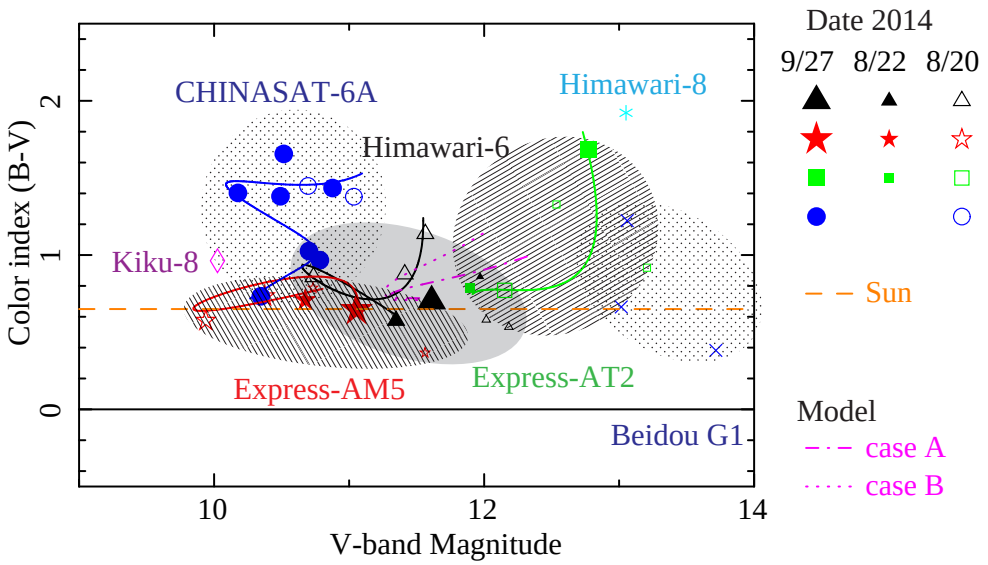

Fig. 8. Color-Magnitude diagram (CMD)

5. CONCLUSION

In order to classify the artificial satellite, we measured in laboratory the surface reflectance of common satellite materials. Before the satellite observation, we calculated visual magnitude of a satellite by simplified calculation model. As a result, we obtained the expected brightness can change the range between 3 and 4 magnitudes in one night, but color index changes only from 1 to 2 magnitudes.

Next, we observed the color photometric data of several GEO satellite visible from Japan using a ground-base telescope. We chose the weather satellite Himawari and the satellites around it as the observation target listed in table 3. In August and September 2014, we obtained the color photometric light curves with the Johnson's B and V bandpass filters.

Although the observation date is a month different, there wasn't dramatic change in the range of magnitudes excluding significant absorption due to clouds. Therefore, we extrapolate the data outside of the observing time, and estimated the color-magnitude diagram (CMD). As a result, color index changed approximately from 0.5 to 1 magnitude in one night, and the order of magnitude was not changed in all cases. We consider that the difference between calculation and observation is caused by (1) the size of the satellites, (2) the geometry of the satellites, and (3) the spectral reflection characteristic of each surface.

We thus confirm that the color index versus the visual magnitude diagram called color-magnitude diagram is quite effective for satellite type estimation. Therefore, the color photometric or the spectroscopic observation is useful for understanding of the GEO satellites.

REFERENCES

1. PAYNE, T. E. et al. Color Photometry of GEO Satellites, Proceedings of Space Control Conference, Vol. 1, 49–54, 1999.
2. BESSEL, M. S. UBVRI passbands , PASP, Vol. 102, 1181-1199, 1990.
3. HASHIMOTO, O. et al. Photometric and spectroscopic observations of geostationary satellites with the use of the 1.5m telescope at Gunma Astronomical Observatory, Spaceguard Research, Vol. 8, 2015.